Biochemical and Biophysical Research Communications 441 (2013) 999–1004

Contents lists available at ScienceDirect

Biochemical and Biophysical Research Communications

journal homepage: www.elsevier.com/locate/ybbrc

Prediction of the interaction between spermidine and the G-G mismatch containing acceptor stem in tRNA^{Ile}: Molecular modeling, density functional theory, and molecular dynamics study

Yoshihiro Hayashi [a,1], Hajime Sugiyama [b,c,1], Akiko Suganami [b,1], Kyohei Higashi [d], Keiko Kashiwagi [e], Kazuei Igarashi [d,f], Susumu Kawauchi [a], Yutaka Tamura [b,*]

[a] Department of Organic and Polymeric Materials, Graduate School of Science and Engineering, Tokyo Institute of Technology, Tokyo 152-8522, Japan
[b] Department of Bioinformatics, Graduate School of Medicine, Chiba University, Chiba 260-8670, Japan
[c] Bio IT Development, Fujitsu Limited, Chiba 261-8588, Japan
[d] Department of Clinical and Analytical Biochemistry, Graduate School of Pharmaceutical Sciences, Chiba University, Chiba 260-8675, Japan
[e] Faculty of Pharmacy, Chiba Institute of Science, Choshi 288-0025, Japan
[f] Amine Pharma Research Institute, Chiba 260-0856, Japan

ARTICLE INFO

Article history:
Received 30 October 2013
Available online 12 November 2013

Keywords:
Density functional theory
Molecular dynamics simulations
Polyamine
Spermidine
tRNA

ABSTRACT

Polyamines, putrescine, spermidine (SPD), and spermine are closely linked to cell growth, and highly regulate the levels of transcription, translation and protein turnover. We propose that SPD stimulates the formation of Ile-tRNA^{Ile} by inducing a selective structural change of the G-G mismatch containing acceptor stem in tRNA^{Ile}. Here, we provide insight into how SPD recognizes and stabilizes the G-G mismatch containing acceptor stem in tRNA^{Ile} with molecular modeling (MM), density functional theory (DFT) calculations, and molecular dynamics (MD) simulations. The results of the MM and DFT calculations indicate that the negatively charged region of the G-G mismatch containing acceptor stem in tRNA^{Ile} is preferentially recognized by positively charged SPD. In addition, MD simulations indicate that all of the positively charged amino groups of SPD under physiological conditions (N1(NH_3^+), N5(NH_2^+), and N10(NH_3^+) could form hydrogen bonds with tRNA^{Ile} and trigger the SPD-induced stabilization and structural change of the G-G mismatch containing acceptor stem in tRNA^{Ile}. Thus, this approach should be useful for determining the preferential binding site and appropriate binding mode of polyamines on tRNA^{Ile}.

1. Introduction

Putrescine (butane-1,4-diamine), spermidine (SPD, N-(3-aminopropyl)butane-1,4-diamine) and spermine (N,N′-bis(3-aminopropyl)butane-1,4-diamine) are low molecular weight, linear, flexible polyamine molecules that are abundant in all prokaryotic and eukaryotic cells [1]. Since polyamines are closely linked to cell growth, inhibitors of polyamine biosynthesis are promoted as antiproliferative agents [2,3]. Many studies have focused on the physiological role of polyamines in a wide array of organisms, and investigated the role of polyamines in therapeutic applications, such as cancer and parasitic or bacterial infection [4]. Polyamines are positively charged under physiological ionic and pH conditions (Fig. 1), and negatively charged cellular macromolecules, such as DNA, RNA and certain proteins, are natural targets for polyamines [5]. The distribution of polyamines in different negatively charged cellular macromolecules, such as RNA/polyamine complexes, in rat liver, bovine lymphocytes, and *Escherichia coli* has been determined in our previous work [6,7]. Moreover, interactions between positively charged polyamines and negatively charged nucleic acids play a crucial role in DNA stabilization and RNA processing, which may affect gene expression, translation, and protein activity [8,9].

We have already reported that polyamines preferentially recognize and bind to double-stranded RNA rather than single-stranded RNA and double-stranded DNA [10]. Furthermore, polyamines have a stabilizing effect on DNA–RNA hybrids, triplex DNA, rRNA, mRNA, and tRNA [11–16]. However, despite these extensive studies, the interactions of polyamines with tRNA are still less well understood than the interactions of polyamines with DNA. Therefore, more specific theoretical and experimental studies of polyamine–tRNA interactions are required [17–20].

Abbreviations: DFT, density functional theory; MD, molecular dynamics; MM, molecular modeling; SPD, spermidine.

* Corresponding author.
E-mail address: yutaka_tamura@faculty.chiba-u.jp (Y. Tamura).

[1] These authors contributed equally to this work.

0006-291X/$ - see front matter © 2013 Elsevier Inc. All rights reserved.
http://dx.doi.org/10.1016/j.bbrc.2013.11.016

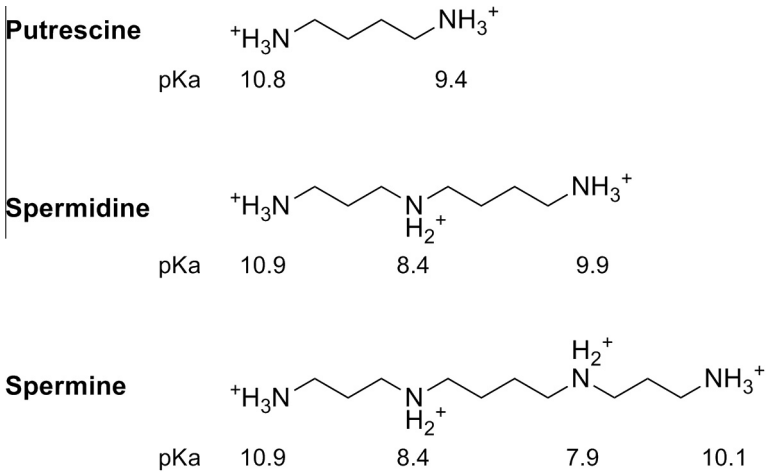

Fig. 1. Chemical structure of polyamines and their pKa values.

Previously, we extensively studied the mechanism of polyamine stimulation of rat liver Ile-tRNA^{Ile} formation [21] and oligopeptide-binding protein (OppA) synthesis [22]. In addition, we have shown that a selective conformational change of the bases in the bulged-out region of double-stranded RNA is caused by polyamines [21]. This can be explained by the ability of polyamines to bind and change the secondary structure of tRNA, mRNA, and rRNA [2,22–25]. Recently, Ouameur et al. reported the preferential binding sites of polyamines on tRNA, and the significance of the tRNA/polyamine complex formation *in vivo* [26]. They proposed several binding models for biogenic polyamines, and their biological significance was discussed. However, the interactions of the biogenic polyamines with tRNA are not still clearly defined [13,14,26].

In this study, we investigated the SPD binding sites and modes in the G-G mismatch acceptor stem in tRNA^{Ile} by molecular modeling (MM), density functional theory (DFT) calculations and molecular dynamics (MD) simulations.

2. Materials and methods

2.1. Molecular modeling

A 22-nucleotide hairpin loop and dangling end containing RNA fragment was used as the model of tRNA^{Ile}, and will be referred to as tRNA^{Ile}-mimic. Molecular modeling (MM) of the structure was based on the canonical A-form duplex of the RNA by HyperChem (version 8, Hypercube, Alberta, Canada). The hairpin loop and dangling end structure from the Brookhaven Protein Databank were then extended using MOE (version 2007, CCG, Montreal, Canada). In the first structure, the initial octameric stem structure was constructed based on a canonical A-form duplex of the RNA 5′-r[GGCCGGU]-3′ and its complementary RNA 3′-r[CCGGCCA]-5′. In the second structure, the hairpin loop 5′-r[UUCG]-3′ on the A-form duplex of the RNAs was used from the data of the hairpin loop structure (PDB ID; 1BGZ). In the third structure, the dangling end 5′-r[ACCA]-3′ at the 3′ end of the A-form duplex of the RNAs was used from the data of the dangling end structure (PDB ID; 1YHQ). In the fourth structure, the G-G mismatch in the A-form duplex was used from the data of the A-form duplex of the RNA structure (PDB ID; 1AMO).

Molecular mechanics calculations using the OPLS-2005 force field were performed in MacroModel (version 8.1, Schrödinger, OR, USA) using the generalized Born/surface area (GB/SA) continuum solvation model. SPD was constructed using the Gaussian 09 program (Gaussian, Inc., CT, USA), and manually docked into tRNA^{Ile}-mimic using HyperChem. The resulting three-dimensional (3-D) structures of SPD, tRNA^{Ile} (PDB ID; 1FFY), and tRNA^{Ile}-mimic were viewed using MOE.

2.2. Density functional theory calculations

Density functional theory (DFT) calculations were performed to examine the electrostatic potential on the tRNA^{Ile}-mimic surface. 3-D structures of tRNA^{Ile}-mimic were obtained from the molecular model described in the previous section. The spatial electrostatic potentials were calculated with the PBE exchange-correlation functional and a DN basis set in DMol3 module of Materials Studio (Accelrys Inc., CA, USA). The surface potentials were displayed using Materials Studio.

2.3. Molecular dynamics simulations

Molecular dynamics (MD) simulations were performed using the AMBER10 package with the AMBER FF02 nucleic acid force field and the modified TIP3P water potential (CONFLEX, Tokyo, Japan). The force field parameters of spermidine were provided by the general amber force field [27], and the partial atomic charges were determined using the RESP method [28] to reproduce the calculated electrostatic potential of a MP2/6-311 + G(3df,3pd)//MP2/6-311G(d,p) calculation using the Gaussian 09 program. The starting structures were placed in a pre-equilibrated solvent box consisting of water and sodium ions, where the number of sodium ions was adjusted to neutralize the systems. The solvent box was extended 8 Å beyond the nucleic acid non-hydrogen atoms. Solvent molecules with non-hydrogen atoms within 1.0 Å of nucleic acid non-hydrogen atoms were deleted. Each system was minimized for 500 adopted basis Newton Raphson (ABNR) steps with mass-weighted harmonic restraints of 2.0 kcal/(mol Å) on the non-hydrogen atoms of the nucleic acid and the ions. MD simulations were performed on the minimized systems for 20 ps in the isochoric-isothermal (NVT) ensemble in the presence of the harmonic restraints on the nucleic acid and the ions. Then, MD simulations were performed on the resulting systems for 2000 ps at 1 atm and 300 K using the isobaric-isothermal (NPT) ensemble. The integration time step was 2 fs, and the SHAKE algorithm was used to constrain all covalent bonds involving hydrogen atoms [29]. The long-range electrostatic interactions beyond the cutoff distance were calculated using the particle mesh Ewald method [30]. The interaction energies between tRNA^{Ile}-mimic and SPD were estimated by the MM-PBSA method [31]. All figures from

the MD simulations of tRNA^{Ile}-mimic/SPD complexes were produced using VMD (http://www.ks.uiuc.edu/Research/vmd/).

3. Results

3.1. Molecular modeling and density functional theory calculations of the G-G mismatch containing acceptor stem in tRNA^{Ile}

To predict and identify the most favorable binding site of spermidine (SPD) in the acceptor stem in tRNA^{Ile}, we used MM and DFT calculations. We have already found that SPD stimulates the formation of Ile-tRNA^{Ile} by inducing a selective structural change of the G-G mismatch containing acceptor stem in tRNA^{Ile} [21]. In a previous study, we used a 22-nucleotide hairpin loop, dangling end, and G-G mismatch containing RNA fragment (Fig. 2a) as a model of tRNA^{Ile}, which was obtained by replacing a 57-nucleotide region in tRNA^{Ile} (8 to 65 in Fig. 2b) with a 4-nucleotide hairpin loop (8 to 11 in Fig. 2a).

In this study, we employed four construction steps as described in Materials and Methods to obtain the appropriate starting structure of tRNA^{Ile}-mimic for the molecular mechanics calculations [32–35]. After the molecular mechanics calculations, we identified the preferable SPD binding site on tRNA^{Ile}-mimic by DFT calculations [36].

Fig. 2c shows that the most negatively charged region (the blue-colored surface) has less than −1.0 H per electron, and is covered on the major groove surface consisting of G5, G6, G14, G15, and G16, which is included with the G-G mismatch between G5 and G14 in tRNA^{Ile}-mimic. According to this result, we propose that the positively charged amino groups of SPD – that is, N1(NH_3^+), N5(NH_2^+), and N10(NH_3^+) – recognize and bind to this negatively charged region on tRNA^{Ile}-mimic.

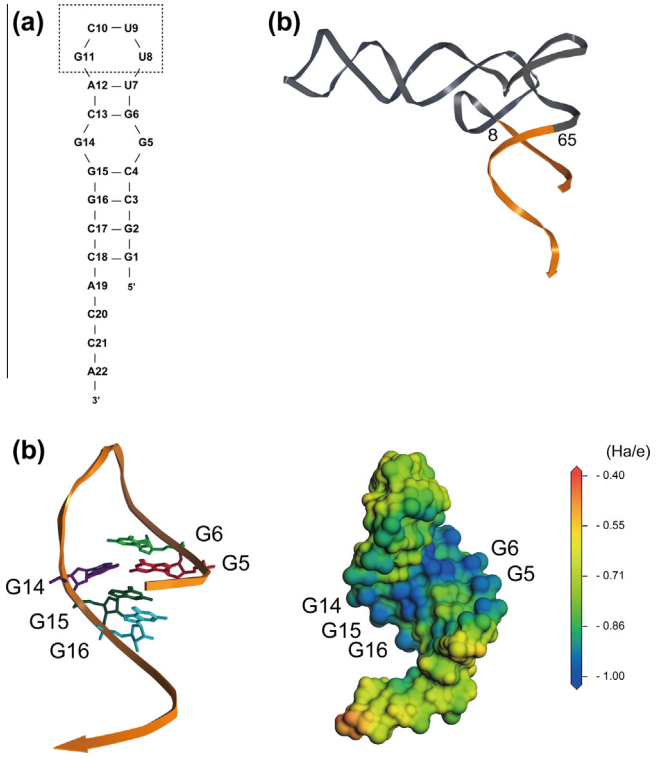

Fig. 2. (a) 2D Structure of the G-G mismatch containing acceptor stem in tRNA^{Ile}-mimic and (b) 3D Structure of tRNA^{Ile}. Orange: acceptor stem region, gray: anticodon, D, and T loop containing region. (c) 3D ribbon and wire model and DFT calculated space-filling model of tRNA^{Ile}-mimic.

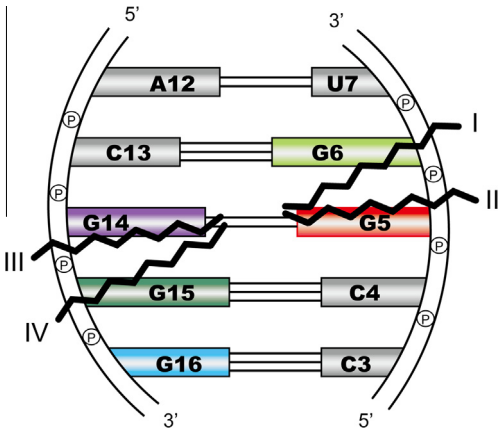

Fig. 3. Four possible orientations of SPD on the G-G mismatch containing acceptor stem in tRNA^{Ile}-mimic. Each orientation contains two opposite directions arising from the asymmetry of SPD.

3.2. Prediction of binding patterns of tRNA^{Ile}-mimic/SPD complexes

To determine the possible orientations of SPD binding to the G-G mismatch containing acceptor stem in tRNA^{Ile}-mimic, we performed manual docking of SPD in the neighborhood of the G-G mismatch between G5 and G14. As we have reported previously, stabilization of the G-G mismatch containing acceptor stem in tRNA^{Ile} is induced by SPD binding to the G-G mismatch region, where irregular hydrogen bonds formed between G5 and G14 [21].

Thus, we determined the four docking modes of SPD to the G-G mismatch region by considering the results of DFT calculations and previous studies [37–39]. In addition, we considered the

Table 1
Interaction energies and hydrogen bond distances between SPD and the G-G mismatch containing acceptor stem in tRNAIle-mimic.

Contacts	Distance (Å)	PBSA energy (kcal/mol)
SPD-Ia–tRNAIle-mimic		
N5–O6 (G6)	3.32	−31.74
N5–O4 (U7) 3.40	3.40	
N10–O2P (G6)	3.09	
SPD-Ib–tRNAIle-mimic		
N10–O6 (G5)	3.16	−30.21
SPD-IIa–tRNAIle-mimic		
N1–O6 (G5)	3.93	
N5–O6 (G6)	3.72	
G6) 3.72	3.57	−33.61
N10–O2P (G5)	3.50	
N10–O2P (G6)	3.32	
SPD-IIb–tRNAIle-mimic		
N1–O2P (G6)	3.15	−30.51
N5–O4 (U7)	3.46	
N10–O6 (G5)	3.27	
SPD-IIIa–tRNAIle-mimic		
N1–O6 (G5)	3.17	−35.77
N1–O6 (G14)	3.83	
N5–O6 (G16)	2.96	
N10–O2P (G14)	3.62	
N10–O2P (G15)	2.91	
SPD-IIIb–tRNAIle-mimic		
N10–O6 (G5)	3.04	−30.99
N10–O6 (G14)	3.60	
SPD-IVa–tRNAIle-mimic		
N1–O6 (G5)	3.14	
N1–O6 (G14)	3.88	−37.40
N5–O6 (G16)	2.92	
N10–O2P (G15)	3.23	
N10–O2P (G16)	2.77	
SPD-IVb–tRNAIle-mimic		
N1–O2P (G15)	3.95	−29.99
N1–O2P (G16)	2.90	

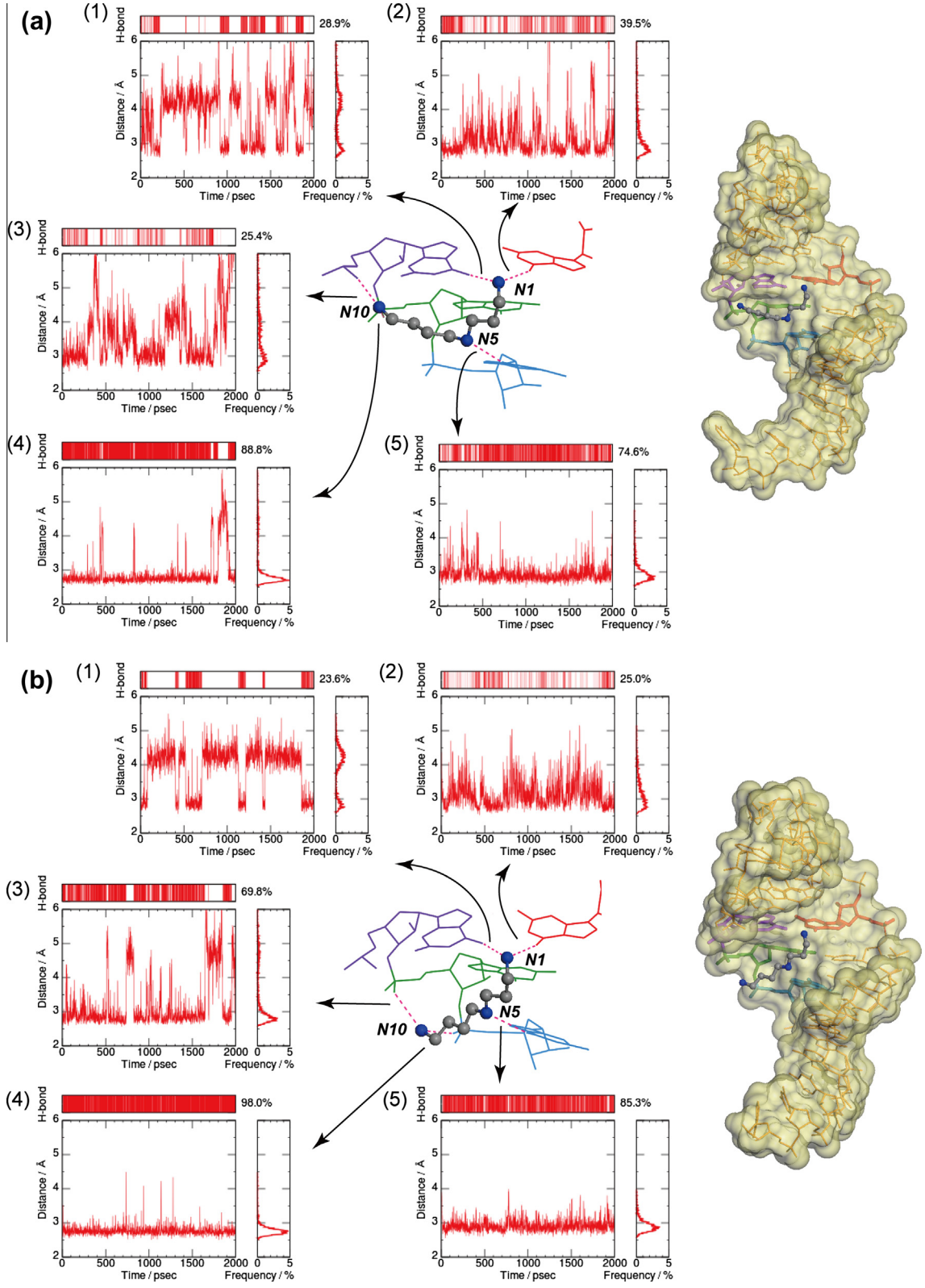

Fig. 4. Variation of the hydrogen bond distances, number of hydrogen bonds, and interaction energies of (a) $tRNA^{Ile}$-mimic/SPD-IIIa and (b) $tRNA^{Ile}$-mimic/SPD-IVa. Red: G5, purple: G14, green: G15, and blue: G16.

asymmetry of SPD. As a result, we used eight SPD binding orientations, including four docking modes due to the asymmetry of SPD, for manual docking in the neighborhood of the G-G mismatch region (Fig. 3).

3.3. Results of MD simulations of the $tRNA^{Ile}$-mimic/SPD complexes

We performed MD simulations on eight $tRNA^{Ile}$-mimic/SPD complexes to obtain the stable binding structures (Fig. S1, Support-

ing Information) [40–45]. We summarize the average bond distances and the interaction energies of the eight $tRNA^{Ile}$-mimic/SPD complexes in Table 1. According to the number of hydrogen bonds formed between SPD and $tRNA^{Ile}$-mimic, we classified the eight $tRNA^{Ile}$-mimic/SPD complexes into two groups. In the first group that includes $tRNA^{Ile}$-mimic/SPD-Ia, -Ib, -IIIb, and -IVb complexes, one or two of the positively charged amino groups of SPD formed hydrogen bonds with $tRNA^{Ile}$-mimic. In the second group that includes $tRNA^{Ile}$-mimic/SPD-IIa, -IIb, -IIIa, and -IVa complexes, all three of the positively charged amino groups of SPD formed hydrogen bonds with $tRNA^{Ile}$-mimic.

Considering the structural change in the acceptor stem in $tRNA^{Ile}$ induced by SPD binding, it is reasonable to conclude that it is favorable to form as many hydrogen bonds as possible between SPD and $tRNA^{Ile}$-mimic. Therefore, it seems sensible to assume that the second group represents the most favorable binding modes of SPD with $tRNA^{Ile}$-mimic. Furthermore, considering the stable PBSA energies (Table 1), we concluded that SPD-IIIa and SPD-IVa are the most favorable binding modes of $tRNA^{Ile}$-mimic/SPD complexes.

3.4. Detailed observations of the docking Mode of $tRNA^{Ile}$-mimic/SPD complexes

To better classify the SPD interactions with $tRNA^{Ile}$-mimic, we analyzed the hydrogen bonds formed in the $tRNA^{Ile}$-mimic/SPD-IIIa and $tRNA^{Ile}$-mimic/SPD-IVa complexes.

All of the intermolecular contact distances between SPD and $tRNA^{Ile}$-mimic were monitored during the course of the 2000 ps MD simulations. We viewed the trajectories of the time versus distance plots for each contact and the corresponding distribution histograms of $tRNA^{Ile}$-mimic/SPD-IIIa (Fig. 4a) and $tRNA^{Ile}$-mimic/SPD-IVa (Fig. 4b) [46]. These results indicate that the $tRNA^{Ile}$ binding sites for SPD-IIIa are O6(G5), O6(G14), O6(G15), and the backbone phosphate groups of G14 and G15 (Fig. 4a). On the other hand, the binding sites for SPD-IVa are O6(G5), O6(G14), O6(G16), and the backbone phosphate groups of G15 and G16 (Fig. 4b).

In the complexes, the hydrogen bond distance of $N5(NH_2^+)$–O6(G16) is about 3.0 Å for both $tRNA^{Ile}$-mimic/SPD-IIIa (Fig. 4a(5)) and $tRNA^{Ile}$-mimic/SPD-IVa (Fig. 4b(5)). In addition, the hydrogen bonds $N5(NH_2^+)$—O6(G16) of $tRNA^{Ile}$-mimic/SPD-IIIa (Fig. 4a(5)) and $tRNA^{Ile}$-mimic/SPD-IVa (Fig. 4b(5)) are present 74.5% and 85.3% of the time, respectively. Moreover, the hydrogen bond distances of $N10(NH_3^+)$—PO_2^-(G15) (Fig. 4a(4)), $N10(NH_3^+)$—PO_2^-(G15) (Fig. 4b(3)), and $N10(NH_3^+)$—PO_2^-(G16) (Fig. 4b(4)) are also about 3.0 Å, and the charge-assisted hydrogen bonds are present 88.8%, 69.8%, and 98.0% of the time during the simulations, respectively. In contrast, the hydrogen bond between N1(G5) and O6(G14) is disturbed if other hydrogen bonds are formed, such as $N1(NH_3^+)$—O6(G5) (Fig. 4a(1) and b(1)) and $N1(NH_3^+)$–O6(G14) (Fig. 4a(2) and b(2)). We presume that the differences in the hydrogen bonding might be due to a selective structural change of $tRNA^{Ile}$.

4. Discussion

Polyamines are small organic polycations found in virtually all prokaryotic and eukaryotic cells. They are closely linked to cell growth, and highly regulate the levels of transcription, translation and protein turnover [1,5]. This is why the negatively charged macromolecules in the cell, such as DNA, RNA, and certain proteins, are natural targets for polyamines [2,47,48].

We already reported the mechanism of polyamine stimulation of $tRNA^{Ile}$ formation and protein synthesis [21,22]. In addition, we showed a selective conformational change of the bases in the bulged-out region of double-stranded RNA by SPD and how SPD recognize and stabilize G-G mismatch containing acceptor stem in $tRNA^{Ile}$ measured with circular dichroism spectroscopy [21]. However, despite many earlier suggestive studies, the preferential binding site and the appropriate binding formation of SPD on tRNA are not yet clarified [13,14,26].

In this study, we have examined the binding sites and modes of SPD on $tRNA^{Ile}$, and estimated the change in the structure of the G-G mismatch acceptor stem in $tRNA^{Ile}$ due to SPD binding. Specifically, we have focused on change in the charge distribution caused by SPD binding to the major groove and evaluated its dynamics with atomistic MD simulations [45]. As a result, we obtained important information about the hydrogen bonding network formation between SPD and $tRNA^{Ile}$, which includes the stability and the conformational change of $tRNA^{Ile}$/SPD complexes [46].

From the binding mode obtained from the MD simulations, we propose the following: (1) $N10(NH_3^1)$ group of SPD recognizes the phosphate group of $tRNA^{Ile}$ with electrostatic interaction by the competition with monovalent and bivalent cations, such as Na^+, K^+, and Mg^{2+}. (2) $N5(NH_2^1)$ of SPD binds to a nucleobase of $tRNA^{Ile}$ by hydrogen bonds, which stabilizes the complex. (3) $N1(NH_3^+)$ of SPD induces a selective structural change of $tRNA^{Ile}$ by the formation of hydrogen bonds, such as $N1(NH_3^1)$–O6(G5) and $N1(NH_3^1)$–O6(G14).

Thus, we could perform a detailed analysis of the interactions between SPD and $tRNA^{Ile}$ through the characterization of the individual hydrogen bonds between SPD and $tRNA^{Ile}$. In summary, the results described in this study have provided information on the mechanism of the interaction between biogenic polyamines and tRNA.

Acknowledgments

We are grateful to Dr. Xia Han and Ms. Satomi Mizuno (Chiba University) for their *in vitro* experimental information. We also thank Dr. Toshio Watanabe (Tokyo Institute of Technology) for his *in silico* technical advice. This study was supported in part by a Research Grant of Futaba Electronics Memorial Foundation to A.S. and Y.T. (No. 10108).

Appendix A. Supplementary data

Supplementary data associated with this article can be found, in the online version, at http://dx.doi.org/10.1016/j.bbrc.2013.11.016.

References

[1] J.-Y. Wang, R.A.J. Casero, Polyamine Cell Signaling, Human Press Inc., Totowa, NJ, 2006.
[2] K. Igarashi, K. Kashiwagi, Polyamines: mysterious modulators of cellular functions, Biochem. Biophys. Res. Commun. 271 (2000) 559–564.
[3] Y. He, T. Shimogori, K. Kashiwagi, A. Shirahata, K. Igarashi, Inhibition of cell growth by combination of α-difluoromethylornithine and an inhibitor of spermine synthase, J. Biochem. 117 (1995) 824–829.
[4] L.J. Marton, A.E. Pegg, Polyamines as targets for therapeutic intervention, Annu. Rev. Pharmacol. Toxicol. 35 (1995) 55–91.
[5] C.W. Tabor, H. Tabor, Polyamines, Annu. Rev. Biochem. 53 (1984) 749–790.
[6] S. Watanabe, K. Kusama-Eguchi, H. Kobayashi, K. Igarashi, Estimation of polyamine binding to macromolecules and ATP in bovine lymphocytes and rat liver, J. Biol. Chem. 266 (1991) 20803–20809.
[7] S. Miyamoto, K. Kashiwagi, K. Ito, S. Watanabe, K. Igarashi, Estimation of polyamine distribution and polyamine stimulation of protein synthesis in *Escherichia coli*, Arch. Biochem. Biophys. 300 (1993) 63–68.
[8] K. Igarashi, K. Kashiwagi, K. Kishida, T. Kakegawa, S. Hirose, Decrease in the S1 protein of 30-S ribosomal subunits in polyamine-requiring mutants of *Escherichia coli* grown in the absence of polyamines, Eur. J. Biochem. 114 (1981) 127–131.
[9] K. Igarashi, K. Kishida, K. Kashiwagi, I. Tatokoro, T. Kakegawa, S. Hirose, Relationship between methylation of adenine near the 3′ end of 16-S

ribosomal RNA and the activity of 30-S ribosomal subunits, Eur. J. Biochem. 113 (1981) 587–593.
[10] K. Igarashi, I. Sakamoto, N. Goto, K. Kashiwagi, R. Honma, S. Hirose, Interaction between polyamines and nucleic acids or phospholipids, Arch. Biochem. Biophys. 219 (1982) 438–443.
[11] L. Jovine, S. Djordjevic, D. Rhodes, The crystal structure of yeast phenylalanine tRNA at 2.0 A resolution: cleavage by Mg(2+) in 15-year old crystals, J. Mol. Biol. 301 (2000) 401–414.
[12] T. Thomas, T.J. Thomas, Polyamines in cell growth and cell death: molecular mechanisms and therapeutic applications, Cell. Mol. Life Sci. 58 (2001) 244–258.
[13] B. Frydman, C. de los Santos, R.B. Frydman, A 13C NMR study of [5,8–13C2] spermidine binding to tRNA and to *Escherichia coli* macromolecules, J. Biol. Chem. 265 (1990) 20874–20878.
[14] L. Frydman, P.C. Rossomando, V. Frydman, C.O. Fernandez, B. Frydman, K. Samejima, Interactions between natural polyamines and tRNA: an 15N NMR analysis, Proc. Natl. Acad. Sci. USA 89 (1992) 9186–9190.
[15] S. Venkiteswaran, V. Vijayanathan, A. Shirahata, T. Thomas, T.J. Thomas, Antisense recognition of the HER-2 mRNA: effects of phosphorothioate substitution and polyamines on DNA.RNA, RNA.RNA, and DNA.DNA duplex stability, Biochemistry 44 (2005) 303–312.
[16] M.A. Xaplanteri, A.D. Petropoulos, G.P. Dinos, D.L. Kalpaxis, Localization of spermine binding sites in 23S rRNA by photoaffinity labeling: parsing the spermine contribution to ribosomal 50S subunit functions, Nucleic Acids Res. 33 (2005) 2792–2805.
[17] B.G. Feuerstein, N. Pattabiraman, L.J. Marton, Spermine–DNA interactions: a theoretical study, Proc. Natl. Acad. Sci. USA 83 (1986) 5948–5952.
[18] B.G. Feuerstein, N. Pattabiraman, L.J. Marton, Molecular dynamics of spermine–DNA interactions: sequence specificity and DNA bending for a simple ligand, Nucleic Acids Res. 17 (1989) 6883–6892.
[19] L. van Dam, N. Korolev, L. Nordenskiold, Polyamine–nucleic acid interactions and the effects on structure in oriented DNA fibers, Nucleic Acids Res. 30 (2002) 419–428.
[20] S. Lindemose, P.E. Nielsen, N.E. Mollegaard, Polyamines preferentially interact with bent adenine tracts in double-stranded DNA, Nucleic Acids Res. 33 (2005) 1790–1803.
[21] K. Higashi, Y. Terui, A. Suganami, Y. Tamura, K. Nishimura, K. Kashiwagi, K. Igarashi, Selective structural change by spermidine in the bulged-out region of double-stranded RNA and its effect on RNA function, J. Biol. Chem. 283 (2008) 32989–32994.
[22] M. Yoshida, D. Meksuriyen, K. Kashiwagi, G. Kawai, K. Igarashi, Polyamine stimulation of the synthesis of oligopeptide-binding protein (OppA). Involvement of a structural change of the Shine-Dalgarno sequence and the initiation codon aug in oppa mRNA, J. Biol. Chem. 274 (1999) 22723–22728.
[23] T. Shimogori, K. Kashiwagi, K. Igarashi, Spermidine regulation of protein synthesis at the level of initiation complex formation of Met-tRNAi, mRNA and ribosomes, Biochem. Biophys. Res. Commun. 223 (1996) 544–548.
[24] R.K. Agrawal, P. Penczek, R.A. Grassucci, N. Burkhardt, K.H. Nierhaus, J. Frank, Effect of buffer conditions on the position of tRNA on the 70 S ribosome as visualized by cryoelectron microscopy, J. Biol. Chem. 274 (1999) 8723–8729.
[25] K. Igarashi, K. Kashiwagi, Polyamine Modulon in Escherichia coli: genes involved in the stimulation of cell growth by polyamines, J. Biochem. 139 (2006) 11–16.
[26] A.A. Ouameur, P. Bourassa, H.A. Tajmir-Riahi, Probing tRNA interaction with biogenic polyamines, RNA 16 (2010) 1968–1979.
[27] J. Wang, R.M. Wolf, J.W. Caldwell, P.A. Kollman, D.A. Case, Development and testing of a general amber force field, J. Comput. Chem. 25 (2004) 1157–1174.
[28] P. Cieplak, J. Caldwell, P. Kollman, Molecular mechanical models for organic and biological systems going beyond the atom centered two body additive approximation: aqueous solution free energies of methanol and N-methyl acetamide, nucleic acid base, and amide hydrogen bonding and chloroform/water partition coefficients of the nucleic acid bases, J. Comput. Chem. 22 (2001) 1048–1057.
[29] J.-P. Ryckaert, G. Ciccotti, H.J.C. Berendsen, Numerical integration of the cartesian equations of motion of a system with constraints: molecular dynamics of n-alkanes, J. Comput. Phys. 23 (1977) 327–341.
[30] T. Darden, D. York, L. Pedersen, Particle mesh Ewald: An N⊕log(N) method for Ewald sums in large systems, J. Chem. Phys. 98 (1993) 10089–10092.
[31] B. Kuhn, P.A. Kollman, Binding of a diverse set of ligands to avidin and streptavidin: an accurate quantitative prediction of their relative affinities by a combination of molecular mechanics and continuum solvent models, J. Med. Chem. 43 (2000) 3786–3791.
[32] H. Ide, H. Shimizu, Y. Kimura, S. Sakamoto, K. Makino, M. Glackin, S.S. Wallace, H. Nakamuta, M. Sasaki, N. Sugimoto, Influence of alpha-deoxyadenosine on the stability and structure of DNA, Thermodynamic Mol. Mech. Stud. Biochem. 34 (1995) 6947–6955.
[33] K.E. Lind, V. Mohan, M. Manoharan, D.M. Ferguson, Structural characteristics of 2′-O-(2-methoxyethyl)-modified nucleic acids from molecular dynamics simulations, Nucleic Acids Res. 26 (1998) 3694–3799.
[34] U.B. Christensen, E.B. Pedersen, Intercalating nucleic acids containing insertions of 1-O-(1-pyrenylmethyl)glycerol: stabilisation of dsDNA and discrimination of DNA over RNA, Nucleic Acids Res. 30 (2002) 4918–4925.
[35] Y. Yamamoto, S. Shuto, Y. Tamura, T. Kodama, S. Hoshika, S. Ichikawa, Y. Ueno, E. Ohtsuka, Y. Komatsu, A. Matsuda, Oligodeoxynucleotides having a loop consisting of 3′-deoxy-4′-C-(2-hydroxyethyl)thymidines form stable hairpins, Biochemistry 43 (2004) 8690–8699.
[36] M. Mori, U. Dietrich, F. Manetti, M. Botta, Molecular dynamics and DFT study on HIV-1 nucleocapsid protein-7 in complex with viral genome, J. Chem. Inf. Model. 50 (2010) 638–650.
[37] J. Ruiz-Chica, M.A. Medina, F. Sanchez-Jimenez, F.J. Ramirez, Fourier transform Raman study of the structural specificities on the interaction between DNA and biogenic polyamines, Biophys. J. 80 (2001) 443–454.
[38] A.A. Ouameur, H.A. Tajmir-Riahi, Structural analysis of DNA interactions with biogenic polyamines and cobalt(III)hexamine studied by Fourier transform infrared and capillary electrophoresis, J. Biol. Chem. 279 (2004) 42041–42054.
[39] H. Sugiyama, T. Kumamoto, A. Suganami, W. Nakanishi, Y. Sowa, M. Takiguchi, T. Ishikawa, Y. Tamura, Insight into estrogenicity of phytoestrogens using in silico simulation, Biochem. Biophys. Res. Commun. 379 (2009) 139–144.
[40] N. Korolev, A.P. Lyubartsev, L. Nordenskiold, A. Laaksonen, Spermine: an "invisible" component in the crystals of B-DNA. A grand canonical Monte Carlo and molecular dynamics simulation study, J. Mol. Biol. 308 (2001) 907–917.
[41] N. Korolev, A.P. Lyubartsev, A. Laaksonen, L. Nordenskiold, On the competition between water, sodium ions, and spermine in binding to DNA: a molecular dynamics computer simulation study, Biophys. J. 82 (2002) 2860–2875.
[42] N. Korolev, A.P. Lyubartsev, A. Laaksonen, L. Nordenskiold, A molecular dynamics simulation study of oriented DNA with polyamine and sodium counterions: diffusion and averaged binding of water and cations, Nucleic Acids Res. 31 (2003) 5971–5981.
[43] Y. Zhu, Y. Wang, G. Chen, Molecular dynamics simulations on binding models of Dervan-type polyamide + Cu(II) nuclease ligands to DNA, J. Phys. Chem. B 113 (2009) 839–848.
[44] J. Romanowska, P. Setny, J. Trylska, Molecular dynamics study of the ribosomal A-site, J. Phys. Chem. B 112 (2008) 15227–15243.
[45] Y. Hashem, P. Auffinger, A short guide for molecular dynamics simulations of RNA systems, Methods 47 (2009) 187–197.
[46] A.C. Vaiana, E. Westhof, P. Auffinger, A molecular dynamics simulation study of an aminoglycoside/A-site RNA complex: conformational and hydration patterns, Biochimie 88 (2006) 1061–1073.
[47] P.B. Dervan, Molecular recognition of DNA by small molecules, Bioorg. Med. Chem. 9 (2001) 2215–2235.
[48] D.R. Boer, A. Canals, M. Coll, DNA-binding drugs caught in action: the latest 3D pictures of drug-DNA complexes, Dalton Trans. (2009) 399–414.